

# The effects of centrifugal force on the stability of axisymmetric viscous flow in a rotating annulus

By SEIJI SUGATA AND SHIGEO YODEN

Department of Geophysics, Kyoto University, Kyoto 606, Japan

(Received 16 October 1990)

Axisymmetric flow in a rotating annulus with differential heating is computed for a high-kinematic-viscosity fluid, such as silicone oil, by numerical integration of the Navier–Stokes equations. Linear stability analysis of the steady axisymmetric flow with respect to a wave perturbation gives a transition curve from the axisymmetric regime to the wave regime; the transition curve is similar to that obtained experimentally by Fein & Pfeffer (1976). However, if we neglect the centrifugal force term, the transition curve is not similar, but it resembles the curve for water (a familiar ‘anvil shape’ in the regime diagram). A dimensionless parameter  $\nu^2(a+b)/8g(b-a)^4$  (where  $a$  and  $b$  are the radii of the inner and outer cylinders,  $d$  the depth of the fluid,  $\nu$  the kinematic viscosity,  $g$  the acceleration due to gravity), which equals the ratio of the centrifugal force to the gravity force divided by the Taylor number, is more fundamental than the Prandtl number in determining the shape of the transition curve.

---

## 1. Introduction

Rotating annulus experiments with horizontal differential heating have been done to investigate the fundamental dynamics of sloping convection (see e.g. Hide & Mason 1975). Several flow regimes appear, which depend mainly on the following dimensionless parameters: Taylor number ( $Ta = 4\Omega^2(b-a)^5/\nu^2d$ ), thermal Rossby number ( $Ro_T = g\alpha\Delta T/\Omega^2(b-a)^2$ ), Prandtl number ( $Pr = \nu/\kappa$ ) and the aspect ratio ( $\Gamma = (b-a)/d$ ), where  $a$  and  $b$  are the radii of the inner and outer cylinders,  $d$  the depth of the fluid,  $g$  the acceleration due to gravity,  $\Omega$  the rotation rate of the annulus,  $\Delta T$  the imposed radial temperature difference,  $\alpha$  the coefficient of volume expansion of the fluid,  $\kappa$  the thermometric diffusivity,  $\nu$  the kinematic viscosity. In a regime diagram plotted in the  $(\log_{10} Ta, \log_{10} Ro_T)$ -plane, axisymmetric flow is found outside the anvil-shaped region (broken line in figure 1) for the case of water ( $Pr = 7.16$ ). Barcilon (1964) obtained the anvil shape for the transition curve separating the axisymmetric regime and the wave regime by adding top and bottom Ekman layers to Eady’s baroclinic instability theory. Introduction of the Ekman-layer friction is necessary to obtain the lower axisymmetric regime at small  $Ta$  and small  $Ro_T$ .

Fein & Pfeffer (1976) did an experiment using two different fluids – mercury ( $Pr = 0.0246$ ) and silicone oil ( $Pr = 63$ ) – and obtained regime diagrams for each fluid. The shape of the transition curve for silicone oil is not an anvil shape, as shown by the heavy solid line in figure 1. It is believed that the Prandtl number is the key parameter to explain the difference between the transition curves. However, an anvil-shaped transition curve is obtained even for the parameters of silicone oil if we

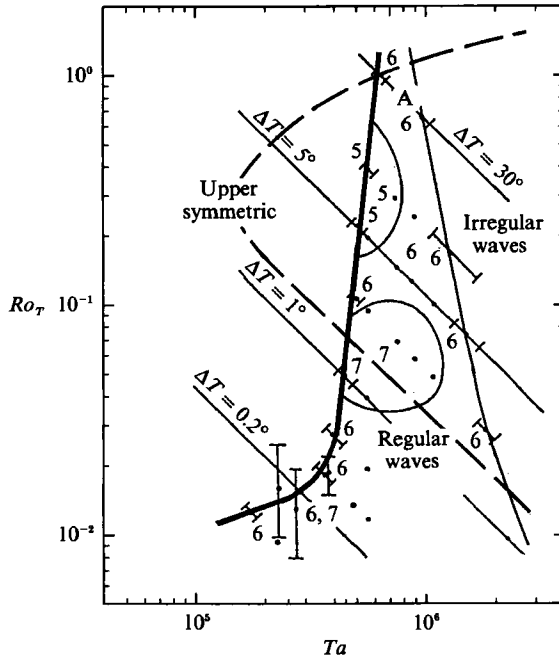


FIGURE 1. Regime diagram for silicone oil (after Fein & Pfeffer 1976). The broken line is the transition curve for water. The numbers indicate the wavenumbers observed in the laboratory experiment.

use Barçilon's model. Fein & Pfeffer suggested the possibility that the slope of the geopotentials due to the centrifugal force, the effects of which are neglected in Barçilon's model, plays a vital role. In the case of silicone oil, the centrifugal force must be about 30 times as large as that for water to get the same Taylor number, because the value of the kinematic viscosity of silicone oil is 5.4 times larger. In order to support their suggestion, they referred to some theoretical studies which take the effects of the slope of the geopotentials into account by sloping the top and bottom boundaries (Hide & Mason 1975). However, simplification and modification of the experimental situations leave some ambiguity.

In this study, we evaluate numerically the effects of the centrifugal force on the transition for silicone oil. We compute steady axisymmetric flow in a two-dimensional parameter space of  $(Ta, Ro_T)$  by time integration of two-dimensional nonlinear Navier–Stokes equations. Linear stability of the axisymmetric flow with respect to wave perturbations is examined as an initial-value problem of the linearized perturbation equations. A transition curve separating the axisymmetric regime and the steady-wave regime is obtained from these linear stability analyses. We then repeat the computation of the axisymmetric flow and the stability analysis without the centrifugal force term. Comparison of the results clarifies qualitative and quantitative differences due to the centrifugal force in an axisymmetric flow, the transition curve and the structure of unstable wave disturbances.

## 2. The model

The governing equations are

$$u_t + uu_r + \frac{vu_\lambda}{r} + wu_z - \frac{v^2}{r} - 2\Omega v = -p_r + \nu \left[ \nabla^2 u - \frac{u}{r^2} - \frac{2v_\lambda}{r^2} \right] + \epsilon \frac{\rho}{\rho_0} r \Omega^2, \quad (1)$$

$$v_t + uv_r + \frac{vv_\lambda}{r} + wv_z + \frac{uv}{r} + 2\Omega u = -\frac{p_\lambda}{r} + \nu \left[ \nabla^2 v - \frac{v}{r^2} + \frac{2u_\lambda}{r^2} \right], \quad (2)$$

$$w_t + uw_r + \frac{vw_\lambda}{r} + ww_z = -p_z + \nu \nabla^2 w - \frac{\rho}{\rho_0} g, \quad (3)$$

$$\theta_t + u\theta_r + \frac{v\theta_\lambda}{r} + w\theta_z = \kappa \nabla^2 \theta, \quad (4)$$

$$\nabla \cdot \mathbf{u} = u_r + \frac{u}{r} + \frac{v_\lambda}{r} + w_z = 0, \quad (5)$$

$$\rho = \rho_0 [1 - \alpha \Delta T \theta], \quad (6)$$

where

$$\nabla^2 = \frac{\partial^2}{\partial r^2} + \frac{1}{r} \frac{\partial}{\partial r} + \frac{1}{r^2} \frac{\partial^2}{\partial \lambda^2} + \frac{\partial^2}{\partial z^2},$$

$(r, \lambda, z)$  are cylindrical coordinates, and  $t$  time. The corresponding velocity components are  $(u, v, w)$ . Dimensionless temperature  $\theta$  is defined as  $\theta \equiv (T - T|_{\text{inner wall}})/\Delta T$ , where  $T$  is the temperature and  $\Delta T$  the imposed temperature difference between the inner and outer cylinders. Density is denoted by  $\rho$ , and  $p$  is pressure divided by the mean density  $\rho_0$ . We modify the traditional Boussinesq approximation by retaining the density variation in the centrifugal force term in the radial momentum equation (1). Parameter  $\epsilon$  is an index of the treatment of the centrifugal force term:  $\epsilon = 1$  when we include the term in the computation, or  $\epsilon = 0$  when we neglect it. Physical parameters of the fluid,  $\nu$ ,  $\kappa$  and  $\alpha$  are assumed to be constant:  $\nu = 5.5 \times 10^{-2} \text{ cm}^2 \text{ s}^{-1}$ ,  $\kappa = 8.8 \times 10^{-4} \text{ cm}^2 \text{ s}^{-1}$  and  $\alpha = 1.05 \times 10^{-3} \text{ K}^{-1}$  for silicone oil.

The size of the annulus and boundary conditions are the same as those in Fein & Pfeffer (1976). The dimensions are  $a = 3.48 \text{ cm}$ ,  $b = 6.02 \text{ cm}$  and  $d = 5.00 \text{ cm}$ . All four bounding surfaces are rigid and the surface of the fluid is in direct contact with the lid. The top and bottom boundaries are thermally insulating. The inner and outer walls are held at different constant temperatures,  $T_a$  and  $T_b$  ( $T_a < T_b$ ), to maintain the difference  $\Delta T$ .

The numerical method developed by Williams (1967*a*) is used to obtain the axisymmetric flow. A stream function  $\psi$  ( $u = -(1/r)\psi_z$ ,  $w = (1/r)\psi_r$ ) and vorticity  $\zeta$  ( $= -\{(1/r)\psi_{zz} + [(1/r)\psi_r]_r\}$ ) are introduced to describe the flow in the vertical  $(r, z)$ -plane. If we adopt the same notation for the finite difference as in Williams (1967*a*), the vorticity equation for the meridional circulation in finite-difference form is

$$\delta_t \zeta + J_A \left( \frac{\zeta}{r} \right) = -g\alpha \Delta T \delta_r \bar{\theta}^{rzz} + 2\Omega \delta_z v^z + \frac{1}{r} \delta_z (v^z)^z + \nu \left[ \delta_{zz} \zeta + \delta_r \left( \frac{1}{r} \delta_r (r\zeta) \right) \right]_{\text{lag}} - \epsilon r \Omega^2 \alpha \Delta T \delta_z \bar{\theta}^z. \quad (7)$$

The last term is an additional term due to the centrifugal force; vertical stratification generates the vorticity. The computed flow is regarded as steady state when variables converge to satisfy the following condition:

$$\left( \frac{\sum_{\text{all grids}} (\partial\theta/\partial t)^2}{\sum_{\text{all grids}} \theta^2} \right)^{\frac{1}{2}} < 10^{-6}. \quad (8)$$

In the linear stability analysis, a small wave perturbation is added to the steady axisymmetric flow:

$$u(r, \lambda, z, t) = U(r, z) + u'(r, z, t) e^{im\lambda}, \quad (9)$$

with corresponding notation for  $v$ ,  $w$ ,  $p$  and  $\theta$ . Substituting these into (1)–(5) and neglecting terms quadratic in the perturbation, we obtain linearized perturbation equations. Following Williams (1969), we integrate the perturbation equations for each wavenumber  $m$  with his staggered grid system. If perturbations of any wavenumber decay with time, the basic axisymmetric flow is stable. On the other hand, it is unstable if at least one of the perturbations grows.

The grid resolution is determined after a convergence test of the solutions. A resolution of  $32(r\text{-direction}) \times 64(z\text{-direction})$  is adopted for  $\Delta T \leq 5$  K and  $64 \times 128$  for  $\Delta T > 5$  K. These grids give equal grid intervals ( $\Delta r = \Delta z$ ) because the aspect ratio of the annulus is 1:2.

We use the temperature difference  $\Delta T$  and the rotation rate  $\Omega$  as controllable experimental parameters, and plot the results on the  $(Ta, Ro_T)$ -plane (a familiar regime diagram like those in figure 1). The dimensional parameters  $\Delta T$  and  $\Omega$  are transformed into the dimensionless parameters  $Ta$  and  $Ro_T$  with the constants  $a$ ,  $b$ ,  $d$ ,  $g$ ,  $\alpha$  and  $\nu$ .

### 3. Results

First, we show the result for the case with the centrifugal force term ( $\epsilon = 1$ ). Figure 2 shows an example of the steady axisymmetric flow of silicone oil obtained at the point marked A in figure 1, where  $\Delta T = 30$  K and  $\Omega = 5.5$  rad s<sup>-1</sup> ( $Ta = 8.46 \times 10^5$ ,  $Ro_T = 0.791$ ). The stream function (figure 2a) shows strong meridional circulation in the boundary layers, which flows counterclockwise and transports heat inward. In the side boundary layers, the temperature field (figure 2b) has a large radial gradient and indicates ‘the overshoot’ of the temperature past its interior value as pointed out by McIntyre (1968). The zonal flow (figure 2c) also has a large vertical shear in the top and bottom boundary layers. In the interior, the meridional circulation is very weak, and the temperature and zonal flow are almost at the thermal wind balance: the buoyancy torque due to the radial temperature gradient is balanced by the Coriolis torque due to the vertical shear of the zonal flow.

Most of these characteristics of the axisymmetric flow are similar to the results for water. Figure 3 is the steady axisymmetric flow for water at the same  $Ta$  and  $Ro_T$  as in figure 2 ( $\Delta T = 5.16$  K and  $\Omega = 1.01$  rad s<sup>-1</sup> for the same annulus). Here the physical parameters of water are:  $\nu = 1.01 \times 10^{-2}$  cm<sup>2</sup> s<sup>-1</sup>,  $\kappa = 1.41 \times 10^{-3}$  cm<sup>2</sup> s<sup>-1</sup> and  $\alpha = 2.06 \times 10^{-4}$  K<sup>-1</sup>. The meridional circulation and the zonal flow are qualitatively similar to those for silicone oil (figure 2). Quantitatively, the intensity of the meridional circulation for silicone oil is about twice that for water. The maximum value of the zonal flow is also about twice as large. Moreover, the thickness of the side

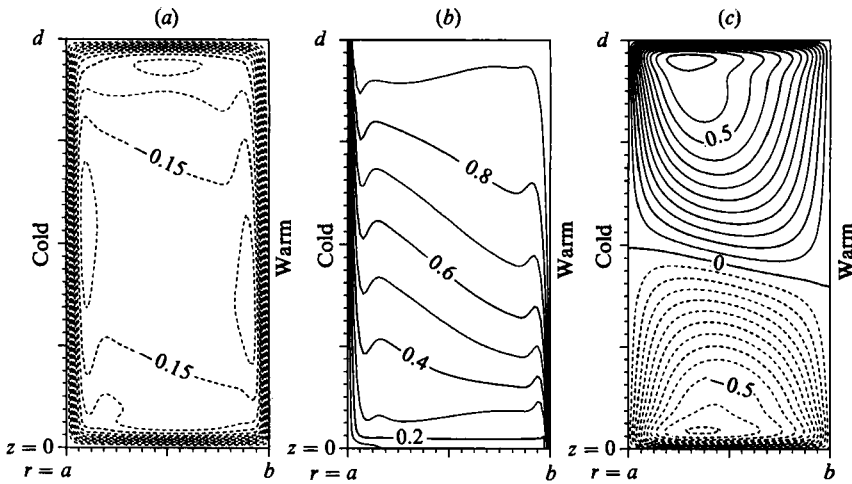


FIGURE 2. Steady axisymmetric flow for silicone oil at  $\Delta T = 30$  K and  $\Omega = 5.5$  rad  $s^{-1}$  ( $Ta = 8.46 \times 10^5$ ,  $Ro_T = 0.791$ ): (a) stream function of meridional circulation ( $cm^3 s^{-1}$ ), (b) normalized temperature and (c) zonal velocity ( $cm s^{-1}$ ). The centrifugal force term is retained in the computations.

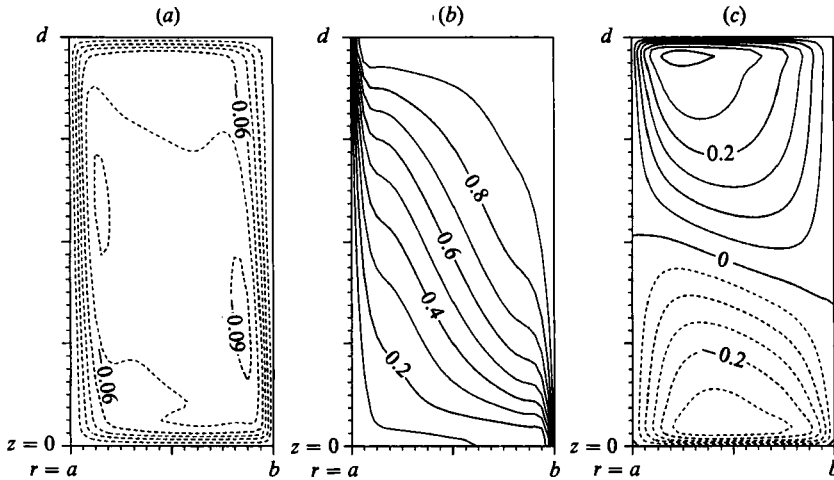


FIGURE 3. As in figure 2 but for water at the same  $Ta (= 8.46 \times 10^5)$  and  $Ro_T (= 0.791)$ , or  $\Delta T = 5.16$  K and  $\Omega = 1.01$  rad  $s^{-1}$ .

boundary layers for water is 1.5–2 times larger than that for silicone oil, although the thickness of the top and bottom boundary layers is almost the same. These are consistent with McIntyre's (1968) estimation of the thickness of the boundary layers: the thickness of the side boundary layers is proportional to  $(\nu\kappa/\alpha \Delta T)^{1/2}$ , and the ratio is 1:1.72 for the present comparison between silicone oil and water. For the top and bottom boundary layers, on the other hand, the thickness of the Ekman layer is proportional to  $(\nu/\Omega)^{1/2}$ , and has the same value for silicone oil and water at the same Taylor number. In the temperature field, the slope of the isotherms in the interior for water is larger than that for silicone oil. Moreover, there is no 'overshoot' of the temperature for water because of the weaker meridional circulation. These characteristics of the temperature field reflect the relative importance of convective

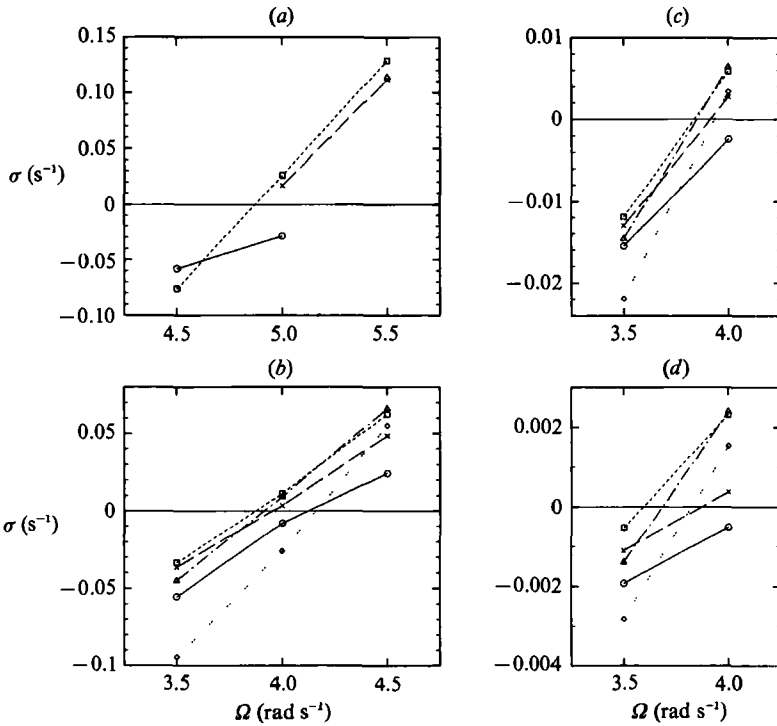


FIGURE 4. Growth rates of wave perturbations as a function of the rotation rate  $\Omega$ . (a)  $\Delta T = 30$  K, (b)  $\Delta T = 5$  K, (c)  $\Delta T = 1$  K and (d)  $\Delta T = 0.2$  K. —○,  $m = 4$ ; ——×,  $m = 5$ ; - - -□,  $m = 6$ ; - · - · -△,  $m = 7$ ; · · · · ·◇,  $m = 8$ .

and conductive transport of heat (Williams 1967 *b*). However, the question of how the temperature distribution is determined for a given external condition remains.

Steady axisymmetric flows are computed for several values of  $\Omega$  at  $\Delta T = 30$  K, 5 K, 1 K and 0.2 K. The lines of constant  $\Delta T$  are the diagonal ones sloping from upper left to lower right in figure 1. A linear stability analysis is done for each steady flow. Time integration of the perturbation equations gives an averaged growth rate  $\sigma$  ( $\text{s}^{-1}$ ) during the time interval  $[t_1, t_2]$ :

$$\sigma \equiv \frac{\log(E(t_2)/E(t_1))}{t_2 - t_1}, \quad (10)$$

where  $E(t)$  is the kinetic energy of the wave perturbation. In this study,  $\sigma$  is calculated after  $\partial E(t)/\partial t$  has attained an almost constant value (or oscillates around a constant value) for more than 30 s.

The growth rate for each wavenumber as a function of the rotation rate  $\Omega$  is shown in figure 4 for (a)  $\Delta T = 30$  K, (b) 5 K, (c) 1 K and (d) 0.2 K. In each figure, the growth rate  $\sigma$  increases with  $\Omega$  and  $\partial\sigma/\partial\Omega$  increases with the wavenumber  $m$ . With a linear interpolation, we can determine a transition point  $\Omega_0$  at which one of  $\sigma$  values becomes positive with increasing  $\Omega$ . For example, in figure 4(a), the axisymmetric flow becomes unstable for the perturbation with  $m = 6$  at  $\Omega_0 = 4.85$   $\text{rad s}^{-1}$ . The absolute value of  $\sigma$  and  $\partial\sigma/\partial\Omega$  become large for large  $\Delta T$  (note that the scale of the ordinate is different among figures 4(a)–4(d)).

We obtain a transition curve joining the transition points in the regime diagram shown in figure 5. The transition curve is very close to the curve obtained

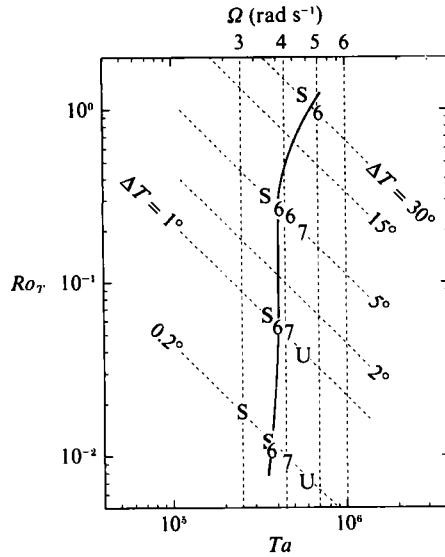


FIGURE 5. Transition curve between the axisymmetric regime and the wave regime obtained from the linear stability analysis. S indicates that the basic flow is stable for perturbations for all wavenumbers computed at the point and U indicates that it is unstable for at least one of the wave perturbations. Each number indicates the most unstable wavenumber.

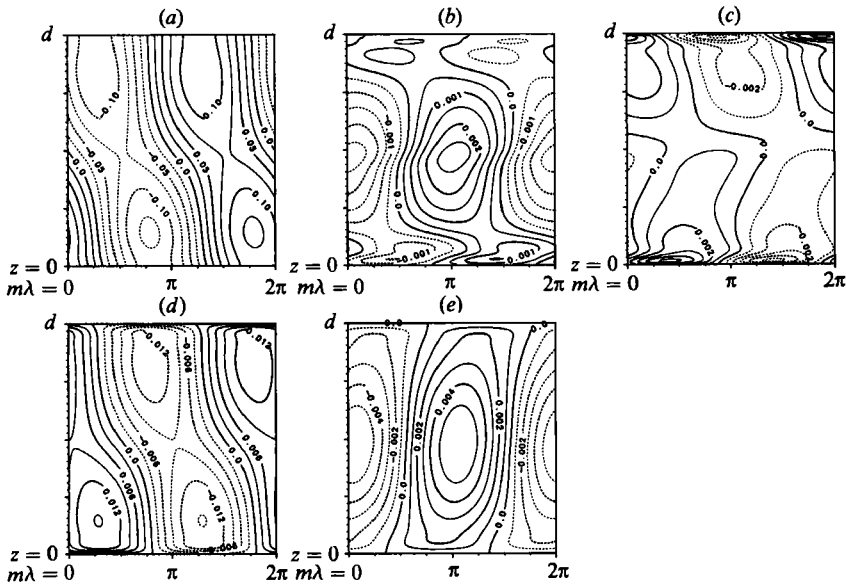


FIGURE 6. Vertical section of the most unstable wave perturbation ( $m = 6$ ) at  $(r-a)/(b-a) = 0.5$  for  $\Delta T = 30$  K and  $\Omega = 5.5$  rad  $s^{-1}$ : (a) pressure, (b) temperature, (c) zonal velocity, (d) radial velocity and (e) vertical velocity.

experimentally for silicone oil (figure 1) except for the region where  $\Delta T \leq 0.2$  K. The perturbation that destabilizes the axisymmetric flow at the transition point has the same wavenumber as observed in the laboratory experiment near the transition curve (figure 1).

The structure of an unstable perturbation is shown in figure 6, which is a vertical-zonal section at the mean radius of the annulus for  $m = 6$  at  $\Delta T = 30$  K and  $\Omega =$

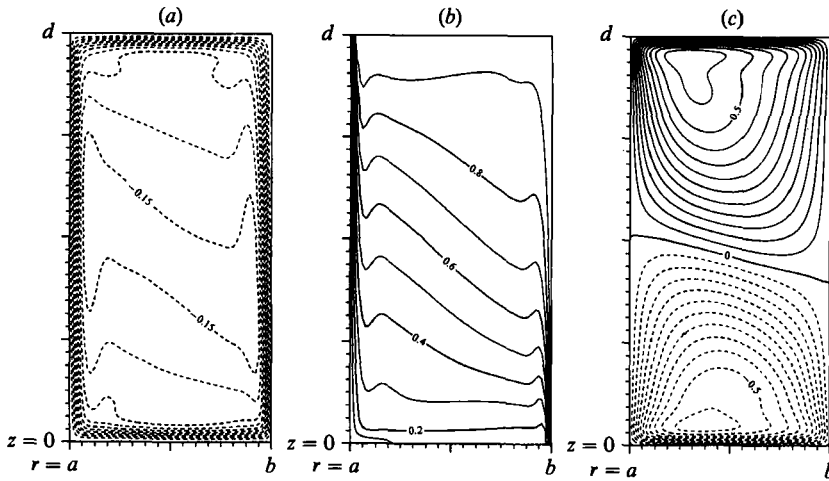


FIGURE 7. As in figure 2 except that the centrifugal force term is neglected in computations.

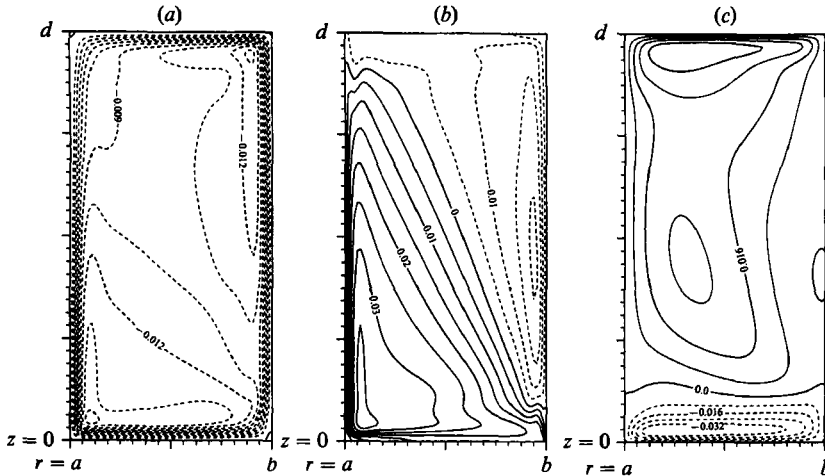


FIGURE 8. Difference of the two steady axisymmetric flows at  $\Delta T = 30$  K and  $\Omega = 5.5$  rad  $s^{-1}$  subtracting the value in figure 7 from that in figure 2. (a) Stream function, (b) normalized temperature and (c) zonal velocity. Units are the same as in figure 2.

$5.5$  rad  $s^{-1}$ . Mutual phase relations of the variables are similar to those obtained for water (Tokioka 1970). The structure is basically that of Eady's wave. However, there is disorder of the structure near the top and bottom boundaries, particularly in the temperature field (figure 6*b*) and the zonal velocity field (figure 6*c*). The disorder near the boundaries is small for small  $\Delta T$ .

In order to investigate the dynamical role of the centrifugal force, we did a calculation neglecting the centrifugal force term ( $\epsilon = 0$ ). Figure 7 shows the steady axisymmetric flow under the same external conditions as in figure 2 ( $\Delta T = 30$  K,  $\Omega = 5.5$  rad  $s^{-1}$ ). The two axisymmetric flows for  $\epsilon = 0$  and  $\epsilon = 1$  are similar to each other: the difference, shown in figure 8, is less than 10%. In the case of  $\epsilon = 1$ , the radial gradient of temperature is weaker and the vertical shear of the zonal velocity is larger. These differences in the temperature and the zonal velocity can be understood by a torque balance in the interior region. When  $\epsilon = 0$ , the buoyancy

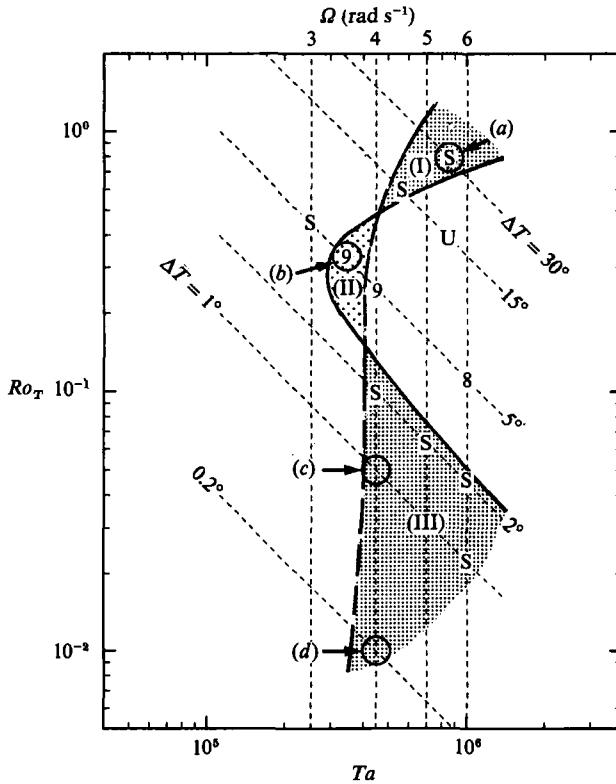


FIGURE 9. As in figure 5 except that the centrifugal force term is neglected in the analysis. The broken line is the transition curve for the case with the centrifugal term (taken from figure 5).

torque (anticlockwise in the  $(r, z)$ -plane) is balanced with the Coriolis torque (clockwise). When  $\epsilon = 1$ , the vertical difference of the centrifugal force due to the density stratification makes an anticlockwise torque. To compensate for the centrifugal torque, it is necessary that the thermally driven torque becomes small and/or the Coriolis torque becomes large.

A linear stability analysis of the axisymmetric flows under  $\epsilon = 0$  gives a transition curve for the case without the centrifugal force (solid line in figure 9). The transition curve has an anvil shape similar to that for water, but its position shifts to large Taylor number compared with that for water (broken line in figure 1). The curve intersects the transition curve for  $\epsilon = 1$  (broken line in figure 9) twice. There are three regions where the stability of the axisymmetric flow is different for the cases of  $\epsilon = 0$  and  $\epsilon = 1$  (shaded regions (I), (II) and (III) in figure 9). In regions (I) and (III), the basic flow is unstable for  $\epsilon = 1$  and stable for  $\epsilon = 0$ . On the other hand, in region (II), it is stable for  $\epsilon = 1$  and unstable for  $\epsilon = 0$ . The structure of unstable wave perturbations is not very different for  $\epsilon = 1$  and  $\epsilon = 0$ .

We further investigate the role of the centrifugal force terms in the equations for axisymmetric flows and wave perturbations. Two additional linear stability analyses are done in the three regions in figure 9: one is a stability analysis of the basic axisymmetric flow with  $\epsilon = 1$  to a wave perturbation with  $\epsilon = 0$ ; and the other is an analysis of the basic flow with  $\epsilon = 0$  to a perturbation with  $\epsilon = 1$ . Table 1 show the result for all these combinations of  $\epsilon$  in the analyses at the four points (a)–(d) in figure 9. At the two points (a) and (b) in regions (I) and (II), the stability depends on the

(a) $\Delta T = 30 \text{ K}, \Omega = 5.5 \text{ rad s}^{-1}$ $Ta = 8.46 \times 10^5, Ro_T = 0.791$			(b) $\Delta T = 5 \text{ K}, \Omega = 3.5 \text{ rad s}^{-1}$ $Ta = 3.43 \times 10^5, Ro_T = 0.326$		
Linear stability			Linear stability		
Basic flow	$\epsilon = 1$	$\epsilon = 0$	Basic flow	$\epsilon = 1$	$\epsilon = 0$
$\epsilon = 1$	unstable	unstable	$\epsilon = 1$	stable	stable
$\epsilon = 0$	stable	stable	$\epsilon = 0$	unstable	unstable
(c) $\Delta T = 1 \text{ K}, \Omega = 4.0 \text{ rad s}^{-1}$ $Ta = 4.47 \times 10^5, Ro_T = 4.98 \times 10^{-2}$			(d) $\Delta T = 0.2 \text{ K}, \Omega = 4.0 \text{ rad s}^{-1}$ $Ta = 4.47 \times 10^5, Ro_T = 9.97 \times 10^{-3}$		
Linear stability			Linear stability		
Basic flow	$\epsilon = 1$	$\epsilon = 0$	Basic flow	$\epsilon = 1$	$\epsilon = 0$
$\epsilon = 1$	unstable	stable	$\epsilon = 1$	unstable	stable
$\epsilon = 0$	unstable	stable	$\epsilon = 0$	unstable	stable

TABLE 1. Results of the stability analysis for combinations of  $\epsilon$  between the computation of the axisymmetric flow and the linear stability analysis

basic axisymmetric flow. The centrifugal force term in the perturbation equations does not change the stability. As shown in figures 2 and 7, the two basic flows for (a) are very similar to each other but the small difference results in different stability; the basic flow in figure 2 is unstable while that in figure 7 is stable. On the other hand, at (c) and (d) in region (III), the stability depends on the perturbation equations. The centrifugal force term in the basic axisymmetric flow does not change the stability. For large  $\Delta T$  the centrifugal force term in the basic axisymmetric flow is important in obtaining a transition curve similar to the experiment, while that term in the perturbation equations is important for small  $\Delta T$ .

#### 4. Discussion

The centrifugal force term has been neglected in previous numerical studies for water (e.g. Williams 1967*a, b*; Tokioka 1970). Since the centrifugal acceleration is much smaller than the gravitational acceleration, it is justified to neglect the centrifugal force term in numerical studies for water. However, in this study, we clarified that the term is necessary for a stability analysis of fluid with large kinematic viscosity. Although it is believed that the Prandtl number is the key parameter, it is not the most appropriate parameter to describe the difference in the shape of the transition curves for water and silicone oil. A transition curve with an anvil shape could be obtained even for fluids with high Prandtl number, if the kinematic viscosity is similar to that of water but the thermometric diffusivity is very small.

Instead of the Prandtl number, a relevant dimensionless parameter is  $\Pi_3 = \Omega^2(b^2 - a^2)/2gd$  (see table 2 in Fowles & Hide 1965). The parameter  $\Pi_3$  is the ratio of the centrifugal force term to the pressure gradient term when we do a scale analysis by assuming geostrophy. In other words,  $\Pi_3$  is the ratio of the centrifugal acceleration to the gravitational acceleration (multiplied by the aspect ratio). If we illustrate the regime diagrams for different fluids in the three-dimensional parameter space ( $Ta$ ,  $Ro_T$ , and a third parameter), as figure 21 in Fein & Pfeffer (1976), it is more appropriate to introduce a dimensionless parameter  $\nu^2(a+b)/8g(b-a)^4 (= \Pi_3/Ta)$  as

the third parameter, because this parameter depends only on the fluid and the apparatus (on the other hand,  $\Pi_3$  depends on  $\Omega$ ). Note that, even for water, large mean radius of the annulus would produce the same effect as for a highly viscous fluid.

## 5. Conclusion

We have done a numerical experiment for sloping convection in a rotating annulus with a highly viscous fluid, such as silicone oil. The centrifugal force terms were retained in the computation because these are not negligibly small for silicone oil. The axisymmetric flows obtained are qualitatively similar to those for water. However, the intensity of the meridional circulation and the zonal flow is larger than that for water at the same  $Ta$  and  $Ro_T$ , while the slope of isotherms in the interior is smaller. A linear stability analysis of the axisymmetric flows with a wave perturbation gives a transition curve similar to that obtained in the laboratory experiment. Moreover, the unstable wavenumber on the transition curve in the linear stability analysis corresponds to that obtained in the laboratory experiment.

Experiments without the centrifugal force term were done to investigate the dynamical role of the term. Axisymmetric flow without the centrifugal force term is not very different from that with the term. However, the transition curve obtained has an anvil shape similar to that for water with low viscosity. The difference in the shape of the transition curve is caused only by a change of the treatment of the centrifugal force term, namely the inclination of the geopotentials due to the centrifugal force strongly affects stability property of the axisymmetric flows. The centrifugal force term must be retained in studying the dynamics of high-kinematic-viscosity fluid.

We further investigated the role of the centrifugal force term in the axisymmetric flow and in the wave perturbation separately. For large  $\Delta T$ , the centrifugal force term in the axisymmetric flow is important in obtaining a transition curve similar to the laboratory experiment. On the other hand, the term in the perturbation equations are important for small  $\Delta T$ .

Fein & Pfeffer (1976) pointed out that the regime diagram depends on the working fluid. Our numerical experiments show the importance of the centrifugal force in determining the transition curve for highly viscous fluids. If we illustrate the regime diagrams for different fluids in the three-dimensional parameter space of the Taylor number, the thermal Rossby number and the third parameter, it is more appropriate to use a dimensionless parameter  $\nu^2(a+b)/8g(b-a)^4$  ( $= \Pi_3/\text{Taylor number}$ ) as the third parameter instead of the Prandtl number.

The authors wish to thank Professor I. Hirota and Dr S. Sakai for their valuable comments during the work. This work was supported in part by Grant-in-Aid for Scientific Research from the Ministry of Education.

## REFERENCES

- BARCILON, V. 1964 Role of the Ekman layers in the stability of the symmetric regime obtained in a rotating annulus. *J. Atmos. Sci.* **21**, 291–299.
- FEIN, J. S. & PFEFFER, R. L. 1976 An experimental study of the effects of Prandtl number on thermal convection in a rotating, differentially heated cylindrical annulus of fluid. *J. Fluid Mech.* **75**, 81–112.

- FOWLIS, W. W. & HIDE, R. 1965 Thermal convection in a rotating annulus of liquid: effect of viscosity on the transition between axisymmetric and non-axisymmetric flow regimes. *J. Atmos. Sci.* **22**, 541–558.
- HIDE, R. & MASON, P. J. 1975 Sloping convection in a rotating fluid. *Adv. Phys.* **24**, 47–100.
- MCINTYRE, M. E. 1968 The axisymmetric convective regime for a rigidly bounded rotating annulus. *J. Fluid Mech.* **32**, 625–655.
- TOKIOKA, T. 1970 A stability of axisymmetric flows in a rotating annulus. *J. Met. Soc. Japan* **48**, 293–314.
- WILLIAMS, G. P. 1967*a* Thermal convection in a rotating fluid annulus: part 1. The basic axisymmetric flow. *J. Atmos. Sci.* **24**, 144–161.
- WILLIAMS, G. P. 1967*b* Thermal convection in a rotating fluid annulus: part 2. Classes of axisymmetric flow. *J. Atmos. Sci.* **24**, 162–174.
- WILLIAMS, G. P. 1969 Numerical integration of the three-dimensional Navier–Stokes equations for incompressible flow. *J. Fluid Mech.* **37**, 727–750.